Atmos. Chem. Phys. Discuss., 14, 32491–32533, 2014
www.atmos-chem-phys-discuss.net/14/32491/2014/
doi:10.5194/acpd-14-32491-2014

Atmospheric Chemistry and Physics Discussions

Turbulence vertical structure of the boundary layer during the afternoon transition

C. Darbieu[1], F. Lohou[1], M. Lothon[1], J. Vilà-Guerau de Arellano[2], F. Couvreux[3], P. Durand[1], D. Pino[4,5], E. G. Patton[6], E. Nilsson[1,7], E. Blay-Carreras[4], and B. Gioli[8]

[1]Laboratoire d'Aérologie, Toulouse, CNRS UMR 5560, Université de Toulouse, Toulouse, France
[2]Meteorology and Air Quality Section, Wageningen University, Wageningen, the Netherlands
[3]CNRM-GAME (Météo-France and CNRS), Toulouse, France
[4]Department of Applied Physics, Universitat Politècnica de Catalunya, BarcelonaTech, Barcelona, Spain
[5]Institute of Space Studies of Catalonia (IEEC-UPC), Barcelona, Spain
[6]National Center for Atmospheric Research, Boulder, Colorado, USA
[7]Uppsala University, Uppsala, Sweden
[8]Institute of Biometeorology – National Research Council (IBIMET-CNR), Florence, Italy

Received: 7 November 2014 – Accepted: 11 November 2014 – Published: 22 December 2014

Correspondence to: C. Darbieu (darc@aero.obs-mip.fr)

Published by Copernicus Publications on behalf of the European Geosciences Union.

ACPD
14, 32491–32533, 2014

Abstract

We investigate the decay of planetary boundary layer (PBL) turbulence in the afternoon, from the time the surface buoyancy flux starts to decrease until sunset. Dense observations of mean and turbulent parameters were acquired during the Boundary Layer Late Afternoon and Sunset Turbulence (BLLAST) field experiment by several meteorological surface stations, sounding balloons, radars, lidars, and two aircraft flying extensively during the afternoon transition. We analyzed a case study based on some of those observations and Large-Eddy Simulation (LES) data focusing on the turbulent vertical structure throughout the afternoon transition.

The decay of turbulence is quantified through the temporal and vertical evolution of (1) the turbulence kinetic energy (TKE), (2) the characteristic length scales of turbulence, (3) the shape of the turbulence spectra. A spectral analysis of LES data, airborne and surface measurements is performed in order to (1) characterize the variation of the turbulent decay with height and (2) study the distribution of turbulence over eddy size.

This study points out the LES ability to reproduce the turbulence evolution throughout the afternoon. LES and observations agree that the afternoon transition can be divided in two phases: (1) a first phase during which the TKE decays with a low rate, with no significant change in turbulence characteristics, (2) a second phase characterized by a larger TKE decay rate and a change spectral shape, implying an evolution of eddy size distribution and energy cascade from low to high wavenumber.

The changes observed either on TKE decay (during the first phase) or on the vertical wind spectra shape (during the second phase of the afternoon transition) occur first in the upper region of the PBL. The higher within the PBL, the stronger the spectra shape changes.

ACPD
14, 32491–32533, 2014

1 Introduction

The transition from a well-mixed convective boundary layer to a residual layer overlying a stable nocturnal layer raises several issues (Lothon et al., 2014), which remain difficult to address from both modeling and observational perspectives. The well mixed convective boundary layer with fully developed turbulence is mainly forced by buoyancy. The afternoon decrease of the surface buoyancy flux leads to the decay of the turbulence kinetic energy (TKE), and a change of the structure of the turbulence, which shows more anisotropy and intermittency. It is important to better understand the processes involved, as they can influence the dispersion of tracers in the atmosphere (e.g., Vilà-Guerau de Arellano et al., 2004; Casso-Torralba et al., 2008), and the development of the nocturnal and daytime boundary layers of the following days (Blay-Carreras et al., 2014).

Turbulence decay has been studied with laboratory experiments (e.g., Monin and Yaglom, 1975; Cole and Fernando, 1998), numerical studies with Large-Eddy Simulations (LES) (e.g., Nieuwstadt and Brost, 1986; Sorbjan, 1997) and observations (e.g., Fitzjarrald et al., 2004; Grant, 1997; Brazel et al., 2005; Fernando et al., 2004). In all of thoses studies, the decay was mainly related to the decrease of the surface buoyancy flux, but with complexity gained with shear-driven boundary layers (Pino et al., 2006; Goulart et al., 2003), which slow the decay. Using LES, Nieuwstadt and Brost (1986) considered a sudden shut off of surface heat flux, and found that turbulence decay occurred within a period of the order of the convective time scale $t_* = z_i/w_*$, where z_i is the planetary boundary layer (PBL) depth, and w_* is the convective velocity scale (Deardorff, 1970). However, different results were obtained if a slower decrease of the forcing surface buoyancy flux is considered with an external time scale τ_f (Sorbjan, 1997; Rizza et al., 2013; Nadeau et al., 2011). If τ_f is large relative to t_*, the turbulence can adjust to the forcing change, in quasi-equilibrium, as noted by Cole and Fernando (1998). This is the case in the mid-afternoon PBL, when t_* is around 10 or 15 min and τ_f is around 2 or 3 h. Sorbjan (1997) found that the TKE decay scales with τ_f/t_*, with

ACPD
14, 32491–32533, 2014

t_* estimated at the start of the decay. But in late afternoon and sunset, t_* starts to increase significantly (until the definition of w_* is put into question at zero buoyancy flux), and turbulence may not be able to adjust to the external change. Consequently, an extensive description of the turbulence structure is needed to better understand this decay process in the PBL.

So, the evolution of the turbulence length scales across the AT has not been addressed extensively, but several studies can be found obtaining diverging results. With fundamental consideration of eddy lifetime, or "turn over" time scale, one may state that smaller eddies will decay earlier than larger eddies (Davidson, 2004). This is one explanation given by Sorbjan (1997), from an LES study, for the increase of the characteristic length scale of the vertical velocity found in the mixed (then residual) layer of the LES. On the contrary, with tethered-balloon observations, Grant (1997) showed that the peak of the vertical velocity spectra shifts to smaller length scales in the surface layer during the evening transition. Finally, Nieuwstadt and Brost (1986) and Pino et al. (2006) found that the length scale of maximum spectral energy of the vertical velocity remained constant during the decay process. Pino et al. (2006) also have shown that the characteristic length scales increase with time for other meteorological variables such as the horizontal wind components, temperature and moisture.

The evolution of the turbulence scales remains unclear and only partly understood. It must be thoroughly investigated whether the scales in the mixed and afterward residual layer really increase or not. Considering the time response and equilibrium aspect mentioned above, and the possible decoupling with height between the stabilizing surface layer and the overlying residual layer, it is also important to consider the vertical structure of turbulence decay, i.e. the evolution of turbulence and scales as a function of height. In the surface layer, one may expect the length scales to decrease, as inferred by Kaimal et al. (1972) from the study of surface-layer spectra evolution with stability during the Kansas experiment.

The numerical studies (e.g., Sorbjan, 1997; Pino et al., 2006) often considered the TKE decay integrated over the entire PBL depth, and observations of the turbulence

ACPD
14, 32491–32533, 2014

decay were made most of the time at surface (Nadeau et al., 2011), but only few observational studies considered the vertical structure of the TKE decay (Grant, 1997, Fitzjarrald et al., 2004 in the afternoon-decaying PBL).

Here we investigate the evolution of the turbulence spectra and scales during the afternoon transition (AT) based on the BLLAST (Boundary Layer Late Afternoon and Sunset Turbulence) dataset, collected during summer 2011 (Lothon et al., 2014). A cloud-free, weak wind day (20 June 2011) is considered to analyze the evolution of the turbulence, from midday to sunset, by using both observations and an LES model. Our analysis aims at (1) evaluating with a complete observations data set the capabilities of the LES to simulate the turbulence structure of the afternoon decay, (2) analyzing the evolution of integral scales, TKE, shape of the spectra in both observations and numerical simulation, and as a function of height.

The article is organized as followed: in the next Section, we present the experimental dataset and describe the case study of the 20 June 2011 through the observations (Sect. 2). In Sect. 3, the LES is presented and evaluated with the observations. Our spectral analysis method, used in both observations and LES, is then described in Sect. 4, before we present and discuss our results (Sect. 5). Concluding remarks are given in Sect. 6.

2 Experimental dataset and case study

The BLLAST experiment took place in the south of France, near the Pyrénées mountain range, during the summer 2011. A set of various observational platforms (aircraft, Remotely Piloted Aircraft Systems, balloons) and continuous measurements (towers, remote sensing) monitored the PBL diurnal evolution, focusing on the AT, in various meteorological regimes. BLLAST experiment provides a unique dataset to investigate the vertical structure of the decaying PBL (see Lothon et al. (2014) for a detailed description of BLLAST objectives and experiment).

ACPD
14, 32491–32533, 2014

The experimental dataset used in this study, the chosen study case and its simulation are now described. Note that the site longitude is around 0.21° E, consequently UTC, very similar to local solar time, is used as the time reference hereafter.

2.1 Experimental dataset

In order to monitor the evolution of the mean structure of the PBL during the AT (and initialize the simulation), we use standard radiosoundings launched every 6 h, from 06:00 to 18:00 UTC, and hourly radiosoundings (Legain et al., 2013) of the low troposphere (up to 3 to 4 km), from 13:00 to 18:00 UTC. The launching sites of the two types of radiosoundings are 4 km apart. The radiosondes measured temperature, water vapour content and the sonde location from which the horizontal wind components are deduced.

Surface energy balance and turbulence structure in the surface layer are provided by several ground stations over different vegetation coverages (wheat, corn, grass, pine forest and moor (composed of heather and gorse)). A permanent 60 m tower, provides integrated turbulence measurements in the surface layer above the heterogeneous surface. The statistical moments are estimated over detrended 30 min periods from 10 Hz raw measurements. The surface heat fluxes are used as surface forcing in the simulation.

Two aircraft, the French Piper Aztec (PA) from SAFIRE (Saïd et al., 2005) and the Italian Sky Arrow (SA) from Ibimet and Isafom (Gioli et al., 2006), flew extensively during the afternoon, at 65 and 40 $m\,s^{-1}$, respectively. They measured temperature, moisture, pressure, CO_2 mixing ratio and 3-D wind at 50 Hz (SA) and 25 Hz (PA) along 25 to 40 km legs stabilized in attitude and altitude. The detailed instrumentation of both aircraft is given in Lothon et al. (2014).

ACPD
14, 32491–32533, 2014

2.2 Case description

20 June 2011 was selected as our case study on the basis of meteorological criteria and data coverage. The synoptic situation was a high pressure system over South-West of France, with a light westerly wind leading to a fair and cloud-free weather.

Figure 1 gives the normalized altitude z/z_i of the stacked legs flown by the aircraft as well as the different launching times of the radiosoundings (the method used for the PBL height (z_i) estimation is discussed later). The two aircraft flew simultaneously, the PA flying above the SA. They flew along west-east parallel legs, at three latitudes and, as shown in Fig. 1, at six heights within the PBL, and two different time periods: the first one from 14:30 to 15:30 UTC, the second one later, from 17:45 to 19:00 UTC. This flight strategy gives access to six heights to study the vertical structure of the turbulence within the PBL.

Figure 2 presents the evolution of the potential temperature (θ) and the wind direction in the PBL at several hours from 05:00 to 18:00 UTC on 20 June 2011. During the day, the PBL warms by about 7 K and the PBL depth z_i grows up to about 1100 m a.g.l. Figure 2a also reveals a warm advection above the PBL between 05:15 and 11:00 UTC, that must be taken into account when simulating. After 11:00 UTC, the lapse rate of θ hardly changes in the free atmosphere, meaning that the temperature advection is very weak.

Figure 2b shows an easterly wind within the PBL, veering to westerly above. The wind intensity remains constant all along the day (not shown): it is weak within the PBL (less than 4 m s^{-1}) and increases with height, up to 10 m s^{-1} at 1500 m.

The water vapour mixing ratio (r) increases from 8 to 10 g kg^{-1} in the PBL until 13:00 UTC and decreases afterward. The temporal evolution of the PBL mean vertical structure is further analysed in Sect. 3.2.

The surface sensible and latent heat fluxes (H and LE, respectively) measured above various vegetation coverages are presented in Fig. 3. The maximum value of H varies from 100–130 W m^{-2} over grass and moor to 450 W m^{-2} over the pine forest. LE shows

ACPD
14, 32491–32533, 2014

much less variability between vegetation coverages, maximum values varying from 250 to 350 $W m^{-2}$. The measurements at 60 m height integrate a large footprint and should give flux estimates of the heterogeneous landscape. As such, H measured at 60 m height is encompassed in all the others and is close to the moor and grass, the dominant vegetation covers over the plateau.

In this study, the AT is defined as the period from the time when the surface buoyancy flux is maximum, to the time where it goes to zero (the surface buoyancy flux is defined as the turbulent vertical transport of vitual potential temperature and is approximated as a linear combination of observed surface sensible and latent heat flux). This period varies according to the surface (Lothon et al., 2014). For the moor coverage, whose surface fluxes will be used to drive the simulation of the 20 June 2011, this period starts at 12:00 UTC and ends at 17:50 UTC, while it ends 20 min earlier when considering H instead of the buoyancy flux. This delay is observed for all the intense observation period (IOP) days of the BLLAST campaign implying that the latent heat flux reaches zero systematically later than the sensible heat flux. Thus the forcing time scale of the surface flux decay τ_f is around 5.8 h for the moor site.

3 LES

As a complementary tool, an LES is initialized with the BLLAST observations to study turbulence decay over an homogeneous and flat surface. The simulation of the 20 June 2011 presented in this study complements Blay-Carreras et al. (2014) and Pietersen et al. (2014) LES studies which also use BLLAST dataset as constraints.

3.1 LES configuration and initilization

The LES code from National Center for Atmospheric Research (Moeng, 1984; Sullivan and Patton, 2011; Patton et al., 2005; Lohou and Patton, 2014) is based on the Boussinesq equations, including conservation laws for momentum, mass and the first

ACPD
14, 32491–32533, 2014

law of thermodynamics. A simulation is initialized with early morning radiosoundings and forced with observed surface heat flux and prescribed advection.

The simulation resolves a domain of 10.24 km × 10.24 km horizontally and 3.072 km vertically, with $\Delta x = \Delta y = 40$ m and $\Delta z = 12$ m of horizontal and vertical resolution, respectively. This results from a compromise between the computation time and three constraints: (1) the domain size and resolution were chosen after a sensitivity study (not shown) so that the LES spectra were able to represent the main characteristics of the observed spectra, (2) the resolution was chosen so that the ratio of z_i to $(\Delta x \times \Delta y \times \Delta z)^{1/3}$ was large enough to ensure that the results are independent of the resolution (Sullivan and Patton, 2011), and, (3) the ratio of Δx to Δz was kept rather small, but with a high enough vertical resolution to correctly represent the entrainment zone (Sullivan and Patton, 2011). The time step evolves during the simulation and is about 1.4 s for fully convective conditions.

The simulation was initialized early in the morning, in order to ensure a fully turbulent convective PBL by the afternoon. The simplified wind, potential temperature and specific humidity initial profiles were deduced from the 05:15 UTC radiosounding. An homogenous surface is considered in the LES with imposed surface fluxes which are those measured at the moor site (Fig. 3).

Vertical profiles of large-scale total (horizontal advection plus subsidence) advections of heat and moisture were hourly prescribed in the simulation and linearly interpolated in between. They were derived from AROME forecast model (horizontal resolution of 2.5 km), using the 16 grid points in a box surrounding the experimental site. This model reveals predominant zonal advection, especially during the morning.

From 05:15 to 10:00 UTC, the temperature advection is important and about $10\,\mathrm{K\,day^{-1}}$ from 500 up to 1500 m (not shown). After 11:00 UTC, it decreases and is negligible in the afternoon. This is consistent with what is observed on the evolution of the potential temperature (Fig. 2a). From sunrise to 14:00 UTC, the moisture advection is about $-10\,\mathrm{g\,kg^{-1}\,day^{-1}}$ from the surface up to 500 m, and about $10\,\mathrm{g\,kg^{-1}\,day^{-1}}$ above. After 14:00 UTC, the moisture advection weakens (not shown).

ACPD
14, 32491–32533, 2014

The data files used to run this case (initial profiles, surface flux and advection profiles) are available on the website of the BLLAST database (http://bllast.sedoo.fr/database).

3.2 Evaluation of the simulated boundary layer

The bracket notation $\langle\psi\rangle$ for any simulated variable ψ is used to represent the 2-D-horizontal average over the LES domain. The same notation is used for the 1-D-horizontal average of the airborne measurements along the legs. For the surface dataset, $\bar{\psi}$ represents the time average notation. For these three types of datasets, the turbulent fluctuations ψ' are defined as deviations from the corresponding mean. For a more fair comparison with the simulated variances, the observed variances are estimated by integration of the spectra over the wavenumber range resolved in the simulation. At last, all the simulated mean vertical profiles are averaged over 30 min and noted for simplicity with the bracket notation $\langle\psi\rangle$, which then indicates both horizontal and temporal average.

The evolution of the simulated θ vertical profiles is compared with observations in Fig. 4a from 05:30 to 17:50 UTC. The simulated θ is close to the observations in the mixed layer (differences lower than 0.1 K) and at the free atmosphere, simulating the observed lapse rate decrease between 05:15 and 11:15 UTC due to the prescribed advection.

Figure 4b presents the evolution of the water vapour mixing ratio. The temporal evolution of r profiles shows a well simulated daily humidification. One can notice a 1 g kg^{-1} drier mixed layer at 13:05 and 17:50 UTC than actually observed.

The horizontal mean wind speed is well reproduced in the simulation during the day: the wind remains weak (about 3 m s^{-1} below 1000 m, see Fig. 4c), and increases with altitude to reach 10 m s^{-1} at 2000 m. No wind forcing is prescribed in the simulation, therefore the observed wind direction change from West to East within the mixed layer between 05:30 and 11:30 UTC is not simulated (Fig. 4d). Whilst the wind speed shear is well simulated, the wind direction shear is evidently underestimated. Consequently,

ACPD
14, 32491–32533, 2014

shear-driven processes (Pino et al., 2006) might not be as important in the simulation as in the observations.

The simulated vertical profiles of the buoyancy flux normalized by the surface buoyancy flux at the start of the AT (Fig. 5) have a quite classical shape until 13:30 UTC with a linear decrease with height and negative flux above $0.8\,z_i$. In the simulation, z_i is estimated as the height of the mixed layer, determined with a threshold on the θ vertical gradient ($0.01\,\mathrm{K\,m^{-1}}$). This method was prefered to the one used for radiosoundings (see below) because of the complex humidity profiles which lead to more fluctuating z_i estimates. However, the difference between these two estimates is less than 50 m. After 13:30 UTC, the upper layer characterized by negative entrainment flux deepens and goes down to $0.6\,z_i$ at 18:00 UTC. During the AT the entrainment rate (ratio of the buoyancy flux at the top of the PBL to the buoyancy flux at surface) remains constant and about −0.13 (not shown). Unfortunately, this value cannot be compared to observations since the fluxes deduced from airborne measurements in the PBL vary substantially at that time, and because of lack of statistics of the large scales in a less and less stationary PBL. Long enough aircraft legs to get accurate statistical moment estimates in convective PBL (Lenschow et al., 1994) are even more relevant during the AT.

The temporal evolution of z_i has been estimated from Ultra High Frequency radar wind profiler (hereafter UHF) and radiosounding measurements and compared to the simulation (Fig. 6). z_i is estimated from UHF as the maximum of the refractive index structure coefficient (Heo et al., 2003; Jacoby-Koaly et al., 2002). From radiosoundings, z_i is estimated as the altitude of the maximum relative humidity below 2500 m (this criterion has been shown to be consistent in time and height during BLLAST experiment, Lothon et al., 2014).

Until 09:00 UTC, the UHF detects the residual layer of the previous day. After 10:00 UTC, z_i increase is similarly depicted by the UHF and radiosoundings, with a maximum value of 1100 m. The simulated PBL grows slower than the observed PBL and reaches 850 m. This discrepancy between observed and simulated z_i (which is

ACPD
14, 32491–32533, 2014

larger than the uncertainty of z_i estimate) might be partly explained by a weaker entrainment effect in the simulation due to a lack of wind shear.

The temporal evolution of the simulated and observed TKE at several heights is presented in Fig. 7. The TKE reads

$$\mathrm{TKE}(z,t) = \frac{1}{2}\left(\sigma_u^2(z,t) + \sigma_v^2(z,t) + \sigma_w^2(z,t)\right), \quad (1)$$

where σ_u^2, σ_v^2 and σ_w^2 are the variances of the horizontal u, v, and vertical w wind components. For a better comparison, simulated and observed TKE are estimated using the wind components variances deduced from the integration of the spectra over the wavenumber range of the simulation. By doing this, the TKE associated to large and small eddies observed, but not simulated or resolved in the LES, is removed from the observed TKE. Even with this method, LES underestimates the observed TKE by a factor sometimes as high as 1.5.

Despite the horizontal heterogeneity linked to orography and the surface heterogeneities which are not taken into account in the LES, the mean evolution of the PBL is well simulated with nevertheless some noticeable differences: a lower development of the PBL height of about 200 m, an underestimated TKE by a factor of 1.5 and a directional wind shear not reproduced. Despite these differences on the main PBL structure, the LES is now used to analyse the turbulence processes occurring during the AT.

4 Spectral analysis method

A broad overview of the turbulent conditions during the afternoon is depicted through the analysis of the TKE temporal evolution at different heights in the PBL.

The energy distribution among the different eddy scales is then studied through a spectral analysis of the vertical velocity w within the entire PBL. The evolution of w spectral characteristics is analyzed by use of an analytical spectral model.

ACPD
14, 32491–32533, 2014

This study focuses on w because simulated and observed w spectra are more easily comparable than the spectra of the horizontal components. Indeed, the horizontal components have significant energy at low wavenumber (large scales) in the observations which can not be represented in our simulated domain.

The choice of the analytical spectra is now discussed since several models exist for convective conditions. Among others, the Kaimal et al. (1972) and Kaimal et al. (1976) formulations were established from Kansas experiment observations for the surface layer and from Minnesota experiment observations for the mixed layer. The von Kàrmàn spectral model (Kàrmàn, 1948) is also widely used for isotropic turbulence. Højstrup (1982) proposed a more generalized model for w spectra up to $z/z_i = 0.5$, based on a stability function from neutral to very unstable conditions. However, many of these analytical models were validated for unstable near surface conditions and most of them are not suitable within the entire convective PBL (Lothon et al., 2009). Among several analytical models tested, the general kinematic spectral model for non-isotropic horizontally homogeneous turbulent field from Kristensen and Lenschow (1989) (named hereafter KL89) is the one which best fits the observed spectra at surface and in the boundary layer acquired during the BLLAST field campaign (not shown). For w, the KL89 model writes:

$$\frac{S_{\mathrm{Kris}}(k)}{\sigma_w^2} = \mathrm{co}\frac{l_w}{2\pi}\frac{1+\frac{8}{3}\left(\frac{l_w k}{a(\mu)}\right)^{2\mu}}{\left(1+\left(\frac{l_w k}{a(\mu)}\right)^{2\mu}\right)^{5/(6\mu)+1}}, \tag{2}$$

where

$$a(\mu) = \pi\frac{\mu\Gamma\left(\frac{5}{6\mu}\right)}{\Gamma\left(\frac{1}{2\mu}\right)\Gamma\left(\frac{1}{3\mu}\right)}, \tag{3}$$

ACPD
14, 32491–32533, 2014

k being the wavenumber along the trajectory of the airplane, or along the west-east axis in the simulation (which is also the mean wind direction in the simulation), and in the mean wind direction for surface measurements. Γ is the gamma function. co is a coefficient which adjusts the amount of energy because σ_w^2 is calculated over a limited range of wavenumbers. This model has two other characteristic parameters: the integral length scale l_w, which is a characteristic scale corresponding to the scales over which w remains correlated with itself (Lenschow and Stankov, 1986), and a sharpness parameter μ, which governs the curvature of the spectra in the region of the peak, between the low wavenumber range and the inertial subrange. The larger μ, the sharper the peak. According to Eq. (2), the KL89 model gives the Kaimal et al. (1972) spectrum for $\mu = 0.5$ and the Kàrmàn (1948) spectrum for $\mu = 1$. It is thus a more generalized model, able to adapt to a larger range of conditions. Note that l_w is related to the wavelength of the energy density maximum (Λ_w) by a monotonic function of μ:

$$\Lambda_w = \left\{ \frac{5}{3}\sqrt{\mu^2 + \frac{6}{5}\mu + 1} - \left(\frac{5}{3}\mu + 1\right) \right\}^{\frac{1}{2\mu}} \frac{2\pi}{a(\mu)} l_w. \quad (4)$$

This model is fit to each observed and LES spectrum, by finding the best [co, l_w, μ] triplet using a logarithmic least squares difference method.

The integral scale of w is usually defined from w autocorrelation function R_w as:

$$L_w = \int_0^\infty R_w(r)\mathrm{d}r, \quad (5)$$

where r is the displacement in space or time. L_w gives an estimate of the horizontal size of the convective thermals in the boundary layer. In this study, L_w is obtained using an integration until the first zero of $R_w(r)$ (Lenschow and Stankov, 1986). It is used here as a reference to which l_w is compared.

For surface-based spectra, 30 min samples are used, which is a good compromise between a sufficient number of eddies and stationary conditions. The spectra based

ACPD
14, 32491–32533, 2014

on the aircraft measurements are calculated on 35 km long legs on average. To ensure consistency between simulated and observed spectra, one-dimensional simulated spectra are considered in the LES. They are calculated along the west-east direction and averaged along the north-south direction. Simulated spectra are estimated above the fourth vertical level (to ensure a negligible contribution of the subgrid scale) and every 96 m in the vertical. The same sampling is used to calculate the autocorrelation functions for L_w estimates.

In order to study the evolution of the spectral slopes in specific domains, the wavenumber range is split into three parts: (1) the low wavenumber range $[0, k_1]$, (2) the region, $[k_1, k_2]$, around the maximum energy density at $k = 2\pi/\Lambda_w$, (3) the inertial subrange $[k_2, \infty]$. The limits are defined here as $k_1 = \pi/\Lambda_w$ and $k_2 = 4\pi/\Lambda_w$.

An important part of the study is to verify the level of agreement between the observed or LES spectra and the KL89 analytical model fit. A quality index of the analytical fit is, therefore, estimated based on the ratio between the observed (respectively LES) spectrum and the analytical spectrum:

$$\mathrm{IQ}_{\mathrm{OBS}} = \frac{1}{N_{\mathrm{OBS}}} \sum_k \left| \log\left(\frac{S_{\mathrm{OBS}}(k)}{S_{\mathrm{KL89}}(k)} \right) \right|, \quad (6)$$

$$\mathrm{IQ}_{\mathrm{LES}} = \frac{1}{N_{\mathrm{LES}}} \sum_k \left| \log\left(\frac{S_{\mathrm{LES}}(k)}{S_{\mathrm{KL89}}(k)} \right) \right|, \quad (7)$$

where S_{OBS} is the spectrum calculated from the observed w, S_{LES} is the spectrum calculated from the simulated w, and S_{KL89} is the analytical spectrum given by Eq. (2) that best fits the observed or simulated spectra. N is the number of k values on which S is defined. The larger $\mathrm{IQ}_{\mathrm{OBS}}$ ($\mathrm{IQ}_{\mathrm{LES}}$), the larger the departure between the observed (simulated) and the analytical spectra. No threshold can be found for these fit quality criteria, therefore values of $\mathrm{IQ}_{\mathrm{OBS}}$ and $\mathrm{IQ}_{\mathrm{LES}}$ in convective conditions (from 12:00 to 14:00 UTC) are used as reference.

Figure 8 presents the normalized spectra of w from both aircraft and simulated data, fitted with the KL89 analytical spectra model. The aircraft (simulated) spectra are calcu-

ACPD
14, 32491–32533, 2014

lated at 15:00 and 18:00 UTC and at $z = 0.6\,z_i$ ($z = 0.6 - 0.75\,z_i$ slice-averaged). This figure shows first, the ability of the simulation to properly reproduce both the energy production domain and the inertial subrange, and second, the ability of the analytical spectral model to fit well the observed and simulated spectra in mid-afternoon convective conditions (15:00 UTC) and at the end of the afternoon (18:00 UTC).

For those two examples, $IQ_{OBS} = 0.11$ and $IQ_{LES} = 0.02$ at 15:00 UTC, and $IQ_{OBS} = 0.10$ and $IQ_{LES} = 0.015$ at 18:00 UTC. In general, the quality index for the observations are about 5 to 10 times larger than for the LES (not shown). This is due to the lack of statistics at large scales in observations, leading to larger fluctations in the spectral density energy for the first domain (low wavenumbers), whereas the LES spectra are averaged along the north-south direction, reducing the variability.

We also found that the quality index for observed and simulated data generally remained constant until 19:00 UTC, except a slight increase of IQ_{LES} for data above $0.6z/z_i$ after 18:30 UTC. This means that the spectra fit is equally reliable throughout the AT, allowing the study of the time evolution of the spectra characteristics from the convective conditions until near neutral conditions. This result should be highlighted in the case of simulated spectra given the overly dissipative nature of the subgrid-scale models in the LES (Meneveau and Katz, 2000).

The spectra changes throughout the AT are already noticeable in Fig. 8: Λ_w shifts toward longer wavelength, the spectra flattens and the inertial subrange slope changes. This is further quantified and discussed in the following section.

5 Results

5.1 TKE decay from surface to PBL top

Most previous studies investigated either vertically integrated simulated TKE over PBL depth, or measured TKE in the surface layer. The TKE decay according to height remains sparsely documented.

ACPD
14, 32491–32533, 2014

Figure 9a shows the evolution of half-hour averaged hourly vertical profile of simulated TKE from 11:30 to 18:30 UTC. The profiles show that TKE decreases within the whole depth of the PBL, but that there is a one-hour delay between the start of the decay at the top and the start at the bottom: at 12:30 UTC, the TKE continues to increase in the lower PBL, while it has started to decrease in the upper part. After 15:30 UTC, the decay is homogeneous over the vertical. This differential TKE decay will be named TKE top-down decay hereafter. This result is consistent with Grimsdell and Angevine (2002) and Lothon et al. (2014) studies which revealed, with remote sensing observations, a decay of TKE dissipation rates from top to bottom. Shaw and Barnard (2002) also studied the decay with Direct Numerical Simulation (DNS), based on a realistic surface flux decay. They found that the turbulence is maintained at the surface relative to upper layers, which they explain with shear at surface.

Turbulence anisotropy (see Fig. 9b), considered here as the ratio of the horizontal to the vertical wind variances, gives highlights on the turbulence structure evolution during the TKE decay. Before 16:30 UTC, turbulence anisotropy remains smaller than 1 in the mid-PBL, which is in agreement with the dominant vertical motion of the convective eddies. In the upper and lower parts of the PBL, turbulence anisotropy is larger than 1, due to small vertical velocity variance close to the surface and the entrainment zone (so called "squashed" turbulence Lothon et al., 2006).

The anisotropy ratio becomes larger than 1 only after 17:30 UTC in the middle of the PBL, but increases close to the top as early as 12:30 UTC. The change in anisotropy, like the TKE, starts early in the upper PBL, with an increasing momentum transfer from vertical to horizontal components during the decay process.

5.2 Spectral analysis

5.2.1 Evolution of the vertical velocity's spectral slopes

The slopes of the simulated and observed spectra are first analyzed because (1) they are key characteristics of the turbulence spectra and, (2) the KL89 spectral model

ACPD
14, 32491–32533, 2014

assumes for $kS(k)$ the theoretical slope of 1 and $-2/3$ for low and high wavenumber range, respectively. The slopes are estimated by linear regression on $kS(k)$ for the wavenumber first and third ranges defined in Sect. 4.

In the low wavenumber range, the slopes of the simulated and near-surface observed spectra are close to the theoretical value of 1 and remain approximately constant during the whole day (see Fig. 10a). The spectral slopes of airborne measurements are steeper than the theory predicts and vary from 1.5 to 2.5. This result illustrates the weak statistical representativity of large scales along aircraft flight leading to scattered spectra slope estimates in this wavenumber range.

In the inertial subrange, both simulated and aircraft data reveal steeper slopes than the theoretical value of $-2/3$, even during the fully convective period (Fig. 10b). The reason for these steeper slopes has not been fully investigated but anisotropy smaller than 1 (Fig. 9b) or the presence of coherent structures could be responsible for this feature. Steeper inertial subrange slopes were previously observed with vertically pointing ground based lidar (Lothon et al., 2009) and with airborne high frequency in situ measurements (Lothon et al., 2007) and would deserve further research. At the end of the afternoon, the slopes consistently flatten in both LES and aircraft data. This flattening appears to behave differently according to height in two ways: (1) it occurs earlier at the top of the PBL (around 16:00 UTC) than in the lower layers (after 17:45 UTC at $0.15\,z_i$), (2) the lower in the PBL, the smaller the flattening. These delayed and reduced changes with decreasing altitude are consistent with the constant $-2/3$ slope during the whole day near the surface.

5.2.2 Characteristic length scales

The integral scale is one of the two spectral characteristics determined from the fit of the KL89 analytical spectral model.

We verified that these integral scale estimates (l_w) were similar to estimates of integral scales (L_w) based on the autocorrelation function (Eq. 5) which is more generally

ACPD
14, 32491–32533, 2014

used. The two methods were found to be consistent with each other and to give similar temporal evolution of integral scale (not shown). Hereafter, only l_w is considered.

The temporal evolution of l_w obtained with aircraft and surface data and with the simulation at different heights, is presented in Fig. 11. At midday, the length scales verify what is found in literature, with a value around 200 m (about $0.2\,z_i$) in the middle of the mixed layer (Lenschow and Stankov (1986) with aircraft observations and Dosio et al. (2005) with LES, among others). Smaller length scales are observed and simulated at the top and at the bottom of the mixed layer because of "squashed" eddies near the interfaces. l_w remains approximately constant until 17:00 UTC, and then increases above $0.15\,z_i$ for both LES and aircraft data. The higher the considered level, the sharper the l_w increase.

Close to surface, l_w remains constant until 17:00 UTC at a value of 10 m, then decreases to 5 m. As expected, the 60 m mast data provide longer l_w than at the surface, but with a large scatter (between 30 and 80 m) making difficult the estimate of l_w tendency with time at that height.

5.2.3 Shape of the spectra

The spectral shape is depicted by the μ sharpness parameter (Eq. 2). Figure 12 shows the temporal evolution of μ that gives the best fit of the spectra for simulation, aircraft and surface data. Above $0.15\,z_i$, μ remains constant at a value of about 2 until 16:00 UTC, aircraft and simulated data giving similar results. Those results are similar to those found by Lothon et al. (2009) with ground-based lidar, who also observed sharper spectra than Kaimal spectra ($\mu = 0.5$) in the middle of the PBL. After 16:00 UTC, μ decreases, meaning that the turbulence spectra flatten during the LAT associated with a broadening of the energy containing wavenumber range above $0.15\,z_i$. On the contrary, close to surface and at 60 m height, $\mu \approx 0.5$ throughout the day, which corresponds to the spectral model from Kaimal et al. (1972) and means that the energy wavenumber range remains large during the LAT. In KL89 analytical model, μ, l_w and Λ_w are linked by Eq. (4) which gives higher Λ_w/l_w for higher μ (Lenschow and Stankov,

ACPD
14, 32491–32533, 2014

1986). Consequently, the decrease of μ associated to an increase of l_w during the LAT implies that Λ_w drifts toward larger eddies (as noticed in Fig. 8) but at a lower rate than l_w.

5.3 Timing of the changes

The previous results illustrate the changes of turbulence characteristics throughout the afternoon according to height. The times when these characteristics start to change are now quantified using the simulation data above $0.15\,z_i$, the tower measurements at 60 m and the near surface moor and corn data. The time of change for a parameter x is noted t_x (Fig. 13). For μ, l_w and the slope, it is the time when the decay rates of these spectra parameters depart from their mean value by more than three times their SD (the decay rates are estimated over 1.5 h and their means and SDs are calculated between noon and 14:00 UTC). Because of the diurnal cycle of the TKE and the horizontal and vertical velocity variances, this method could not be applied to determine the time change of these parameters. t_{TKE}, $t_{\langle w'^2\rangle}$ and $t_{\langle u'^2\rangle+\langle v'^2\rangle}$ were thus the time when the decaying rate of the parameter (estimated by linear regression over 1.5 h) becomes larger than an arbitrary threshold of $-0.02\,\mathrm{m^2\,s^{-3}}$.

As already noticed in Sect. 5.1, the TKE first decreases at the top of the boundary layer half an hour after the start of the AT (Fig. 13). This decrease propagates from z_i downward towards the lower layers (down to $0.15\,z_i$) within the following hour. The TKE decrease is exclusively driven by the vertical velocity variance, which decreases at the top of the PBL one and half hour before the maximum of the surface buoyancy flux. The early decrease of the vertical velocity variance is counter-balanced in TKE by the delayed change of the horizontal wind variance. This implies an increase in the anisotropy of the velocity variances in the early stage of surface flux decrease.

The change in other spectral parameters (length scale, sharpness and slope) is observed much later, during the last two hours before the zero surface buoyancy flux. The vertical profiles of t_{l_w}, t_{slope} and t_μ, indicate a flattening and a shift of the spectra toward

ACPD
14, 32491–32533, 2014

the small wavenumbers, with a flattening of the inertial subrange slope, appearing first at the top of the boundary layer and rapidly propagating toward the lower layers.

Near the surface and at 60 m, a very weak evolution of the spectra is observed. The spectra keep the same sharpness, similar to Kaimal spectra, with a constant slope of $-2/3$ in the inertial subrange, and a very slightly decreasing l_w. These results are consistent with the spectra behavior above $0.15\,z_i$. Indeed, μ decreases from around 2 in convective conditions to 0.5 at the end of the AT in the whole upper layer and the l_w increase in the upper layers is less and less pronounced with decreasing height.

5.4 Discussion

The above analysis of the evolution of the turbulence structure during the AT suggests us to separate this period in two stages: early and late afternoon.

In the early afternoon, from the occurrence of the buoyancy maximum until about two hours before sunset, (1) the TKE decreases within the whole PBL, with a one-hour delay between the upper part (earlier decay) and the lower part of the PBL (postponed decay), (2) the vertical profile of anisotropy does not change much within the PBL, except close to the top, and (3) the spectra maintain the characteristics of the fully-developed convective boundary layer, with similar integral scales and sharpness parameter.

In the late afternoon, from two hours before sunset until when the surface buoyancy flux reduces to zero, (1) the TKE decreases more rapidly than during the early AT within the whole PBL, (2) turbulence anisotropy increases abruptly within the PBL, starting initially near the PBL top, and (3) the shape of the spectra evolves, with a decrease of the sharpness parameter, a flattening of the inertial subrange slope, an increase of the integral length scales in the mid and upper PBL. The higher in the PBL, the stronger the increase of the integral scales, with very slight changes of the spectra shape observed close to the surface.

Our understanding of the two different stages of the AT is that during the early afternoon, the buoyancy flux remains large and its decay is slow enough, to give time

ACPD
14, 32491–32533, 2014

to the PBL to adjust to the change and to remain in quasi-steady balance. In other words, the convective time scale t_* is small enough (~ 9 min) relative to τ_f (~ 5.8 h), to allow this quasi-steady state. The spectral characteristics remain similar to what they are at maximum surface buoyancy flux. Buoyancy remains a dominant influence during this stage, which leaves predominance to the vertical velocity variance and convective structures. The latter, with a characteristic horizontal length typically linked to the PBL depth, could maintain a sharp spectral peak. Predominance of convective structures might also be at the origin of the steep inertial subrange slope. Close to surface, where these convective structures are not yet well shaped, inertial subrange slope is $-2/3$.

On the contrary, during the late AT, t_* increases (about 20 min at 17:00 UTC) and the buoyancy flux gets too small for the PBL to maintain the vertical consistency of the turbulence structure from surface up to the top of the PBL. The impact of surface buoyancy decreases faster than that of entrainment during this period: although the entrainment flux magnitude diminishes, entrainment occurs over a broader vertical depth extending down to $0.6\,z_i$ (Fig. 5).

An increase of the entrainment role could explain the increase of the vertical velocity integral scales (Lohou et al., 2010 and Canut et al., 2010) which is observed in the upper PBL during the late afternoon during our BLLAST case. The vertical velocity integral scales increase is consistent with the results of Sorbjan (1997) but differs from those of Pino et al. (2006). This could be due to the progressive cease of the surface flux in Sorbjan (1997) and Grant (1997), vs. the sudden shut-off in Pino et al. (2006). In the surface layer, the decrease of the integral scales is consistent with the observations made by Grant (1997) and with the results of Kaimal et al. (1972).

The flattening observed in the inertial subrange during the late afternoon is difficult to explain because one could expect a steeper slope in inertial subrange when the flow becomes less turbulent, assuming that the smaller scales will dissipate faster than the larger scales. However, hypotheses could be made to explain the observed flattening of the spectra in inertial subrange: (1) the increase of anisotropy might be associated with such change of the cascade, (2) if the turbulence is now freely decaying, without

ACPD
14, 32491–32533, 2014

influence of coherent structures and vertical velocity dominancy, the cascade could become more efficient, resulting in flattening slope according to Moeng and Wyngaard (1988). In any case, it seems that with the turbulence being no longer fully forced, the criteria for locally isotropic turbulence are no longer met.

The progressive shut-off of the surface heat fluxes is shown to be an important aspect of the AT. Nieuwstadt and Brost (1986) and Pino et al. (2006) who analyzed simulations with a sudden shut-off of the buoyancy flux pointed out what they called a demixing process which infers a negative buoyancy flux within the whole PBL. The impact of entrainment in that case might be overestimated. Similar to Sorbjan (1997), when progressively transitioning through the afternoon from surface buoyancy dominated to entrainment dominated regime, the demixing process is strongly reduced and limited to the half-upper part of the PBL.

One might wonder whether these results could be impacted by the initial conditions. The use of all the airborne measurements acquired during the BLLAST experiment shows the general trend of an increasing integral scale during the LAT (not shown). However, it would be useful to complete this study with some additional simulations either targeting other BLLAST IOPs or performing some sensitivity analyses. Wind shear could be particularly under focus as Nieuwstadt and Brost (1986) and Pino et al. (2006) found that strong wind shear at the top and bottom of the PBL delays the decay.

6 Conclusions

This study is based on the use of analytical spectra to depict and quantify changes in the vertical velocity spectra throughout the AT and according to height. BLLAST aircraft and surface station measurements are used to study the turbulence spectral evolution on 20 June 2011. A Large-Eddy Simulation constrained by observed conditions during BLLAST, but further simplified, allows us to investigate a continuous spectra analysis in time and height.

ACPD
14, 32491–32533, 2014

The simulated data, even with simplified forcings and initial conditions, are in a satisfactory agreement with the airborne, radiosonde and surface observations. The model reasonably simulates the turbulence structure through the afternoon with a resolution and a domain size allowing a good fit of the simulated spectra with the Kristensen and Lenschow (1989) analytical model above $0.15 z_i$.

Two main conclusions can be drawn from this study, giving essential highlights on the turbulence evolution in time and height:

(1) This study shows for the first time the different steps occurring during the AT, which is defined as the period starting at the maximum surface buoyancy flux and ending when the buoyancy flux reaches zero. The early afternoon (first phase from 0 to $0.75\,\tau_f$) is characterized by a low-rate decrease of the energy level, but the turbulence characteristics remain similar to those during fully convective conditions: similar turbulence length scales and cascade characteristics from large to small eddies. During the late afternoon (second phase from 0.75 to $1\,\tau_f$), TKE decay rates increase and turbulence characteristics evolve rapidly implying very different eddy size and energy transfer.

(2) The second important point concerns the turbulence evolution along the vertical. The changes observed either on TKE decay (during the early afternoon) or on w spectral shape (during the late afternoon) start at the top of the boundary layer. Furthermore, the higher within the PBL the stronger the spectra shape changes. These results show that the top of the boundary layer is first affected by the changes which migrate downward towards the surface.

Acknowledgements. The BLLAST field experiment was made possible thanks to the contribution of several institutions and supports: INSU-CNRS (Institut National des Sciences de l'Univers, Centre national de la Recherche Scientifique, LEFE-IMAGO program), Météo-France, Observatoire Midi-Pyrénées (University of Toulouse), EUFAR (EUropean Facility for Airborne Research) BLLATE-1&2, COST ES0802 (European Cooperation in the field of Scientific and Technical) and the Spanish MINECO projects CGL2009–08609, CGL2012–37416–C04–03, and CGL2011-13477-E. The field experiment would not have occurred without the contribution of all participating European and American research groups, which all have contributed

ACPD
14, 32491–32533, 2014

in a significant amount. The Piper Aztec research airplane is operated by SAFIRE, which is a unit supported by INSU-CNRS, Météo-France and the French Spatial Agency (CNES). BLLAST field experiment was hosted by the instrumented site of Centre de Recherches Atmosphériques, Lannemezan, France (Observatoire Midi-Pyrénées, Laboratoire d'Aérologie). Its 60 m tower is partly supported by the POCTEFA/FLUXPYR European program. BLLAST data are managed by SEDOO, from Observatoire Midi-Pyrénées. Since 2013, the French ANR supports BLLAST analysis. See http://bllast.sedoo.fr for all contributions. We particularly thank Eric Pardyjak, Oscar Hartogensis, Dominique Legain, and Frédérique Saïd, for providing the surface measurements used in this study. We are also grateful to Bruno Piguet for the first processing of the Piper Aztec dataset and to Dominique Legain and the CNRM-4M team for the frequent radiosoundings. Computer facilities for the Large Eddy Simulation were provided by CALMIP (Calcul en Midi-Pyrénées, France).

References

Blay-Carreras, E., Pino, D., Vilà-Guerau de Arellano, J., van de Boer, A., De Coster, O., Darbieu, C., Hartogensis, O., Lohou, F., Lothon, M., and Pietersen, H.: Role of the residual layer and large-scale subsidence on the development and evolution of the convective boundary layer, Atmos. Chem. Phys., 14, 4515–4530, doi:10.5194/acp-14-4515-2014, 2014. 32494, 32499

Brazel, A., Fernando, H., Hunt, J., Selover, N., Hedquist, B., and Pardyjak, E.: Evening transition observations in Phoenix, Arizona, J. Appl. Meteorol., 44, 99–112, 2005. 32494

Canut, G., Lothon, M., Saïd, F., and Lohou, F.: Observation of entrainment at the interface between monsoon flow and the Saharan Air Layer, Q. J. Roy. Meteor. Soc., 136, 34–46, 2010. 32513

Casso-Torralba, P., Vilà-Guerau de Arellano, J., Bosveld, F., Soler, M., Vermeulen, A., Werner, C., and Moors, E.: Diurnal and vertical variability of the sensible heat and carbon dioxide budgets in the atmospheric surface layer, J. Geophys. Res., 113, D12119, doi:10.1029/2007JD009583, 2008. 32494

Cole, G. and Fernando, H.: Some aspects of the decay of convective turbulence, Fluid Dyn. Res., 23, 161–176, 1998. 32494

ACPD
14, 32491–32533, 2014

Davidson, P.: Turbulence: An Introduction for Scientists and Engineers, Oxford University Press Inc., New York, 2004. 32495
Deardorff, J.: Convective velocity and temperature scales for the unstable planetary boundary layer and for Rayleigh convection, J. Atmos. Sci., 27, 1211–1215, 1970. 32494
Dosio, A., Vilà-Guerau De Arellano, J., and Holtslag, A. A. M.: Relating Eulerian and Lagrangian statistics for the turbulent dispersion in the atmospheric convective boundary layer, J. Atmos. Sci., 62, 1175–1191, 2005. 32510
Fernando, H., Princevac, M., Pardyjak, E., and Data, A.: The decay of convective turbulence during evening transition period, in: 11th Conference on Mountain Meteorology and MAP Meeting, Bartlett (NH), USA, paper 10.3, 2004. 32494
Fitzjarrald, D. R., Freedman, J. M., Czikowsky, M. J., Sakai, R. K., and Moraes, O. L. L.: Momentum and scalar transport during the decay of CBL turbulence, 16th AMS Symposium on boundary layers and turbulence, 2004. 32494, 32496
Gioli, B., Miglietta, M., Vaccari, F. P., Zaldei, A., and De Martino, B.: The sky arrow ERA, an innovative airborne platform to monitor mass, momentum and energy exchange of ecosystems, Ann. Geophys., 49, 109–116, 2006, http://www.ann-geophys.net/49/109/2006/. 32497
Goulart, A., Degrazia, G., Rizza, U., and Anfossi, D.: A theoretical model for the study of convective turbulence decay and comparison with large-eddy simulation data, Bound.-Lay. Meteorol., 107, 143–155, 2003. 32494
Grant, A. L. M.: An observational study of the evening transition boundary-layer, Q. J. Roy. Meteor. Soc., 123, 657–677, 1997. 32494, 32495, 32496, 32513
Grimsdell, A. W. and Angevine, W. M.: Observations of the afternoon transition of the convective boundary layer, J. Appl. Meteorol., 41, 3–11, 2002. 32508
Heo, B., Jacoby-Koaly, S., Kim, K., Campistron, B., Bénech, B., and Jung, E.: Use of the Doppler spectral width to improve the estimation of the convective boundary layer height from UHF wind profiler observations, J. Atmos. Ocean. Tech., 20, 408–424, 2003. 32502
Højstrup, J.: Velocity spectra in the unstable planetary boundary layer, J. Atmos. Sci., 39, 2239–2248, 1982. 32504
Jacoby-Koaly, S., Campistron, B., Bernard, S., Bénech, B., Ardhuin-Girard, F., Dessens, J., Dupont, E., and Carissimo, B.: Turbulent dissipation rate in the boundary layer via uhf wind profiler doppler spectral width measurements, Bound.-Lay. Meteorol., 103, 361–389, 2002. 32502

ACPD
14, 32491–32533, 2014

Kaimal, J., Wyngaard, J., and Coté, O.: Spectral characteristics of surface layer turbulence, Q. J. Roy. Meteor. Soc., 98, 653–689, 1972. 32495, 32504, 32505, 32510, 32513
Kaimal, J., Wyngaard, J., Haugen, D., Coté, O., and Izumi, Y.: Turbulence structure in the convective boundary layer, J. Atmos. Sci., 33, 2152–2169, 1976. 32504
Kàrmàn, T.: Progress in the statistical theory of turbulence, P. Natl. Acad. Sci. USA, 34, 530–539, 1948. 32504, 32505
Kristensen, L. and Lenschow, D. H.: The spectral velocity tensor for homogeneous boundary-layer turbulence, Bound.-Lay. Meteorol., 47, 149–193, doi:10.1177/1553350614532679, 1989. 32504, 32515
Legain, D., Bousquet, O., Douffet, T., Tzanos, D., Moulin, E., Barrie, J., and Renard, J.-B.: High-frequency boundary layer profiling with reusable radiosondes, Atmos. Meas. Tech., 6, 2195–2205, doi:10.5194/amt-6-2195-2013, 2013. 32497
Lenschow, D. H. and Stankov, B. B.: Length scales in the convective boundary layer, J. Atmos. Sci., 43, 1198–1209, 1986. 32505, 32510
Lenschow, D. H., Mann, J., and Kristensen, L.: How long is long enough when measuring fluxes and other turbulence statistics?, J. Atmos. Ocean. Tech., 11, 661–673, 1994. 32502
Lohou, F. and Patton, E. G.: Surface energy balance and buoyancy response to shallow cumulus shading, J. Atmos. Sci., 71, 665–682, doi:10.1175/JAS-D-13-0145.1, 2014. 32499
Lohou, F., Saïd, F., Lothon, M., Durand, P., and Serça, D.: Impact of boundary-layer processes on near-surface turbulence within the West African Monsoon, Bound.-Lay. Meteorol., 136, 1–23, doi:10.1007/s10546-010-9493-0, 2010. 32513
Lothon, M., Lenschow, D., and Mayor, S.: Coherence and scale of vertical velocity in the convective boundary layer from a Doppler lidar, Bound.-Lay. Meteorol., 121, 521–536, doi:10.1007/s10546-006-9077-1, 2006. 32508
Lothon, M., Lenschow, D. H., and Schanot, A.: Status-reminder report on C-130 air-motion measurements. Test of DYCOMS-II new datasets, Internal report, NCAR-RAF, available at: https://www.eol.ucar.edu/raf/Projects/DYCOMS-II/DYCOMS.report1_win07.pdf, 2007. 32509
Lothon, M., Lenschow, D., and Mayor, S.: Doppler lidar measurements of vertical velocity spectra in the convective planetary boundary layer, Bound.-Lay. Meteorol., 132, 205–226, doi:10.1007/s10546-009-9398-y, 2009. 32504, 32509, 32510
Lothon, M., Lohou, F., Pino, D., Couvreux, F., Pardyjak, E. R., Reuder, J., Vilà-Guerau de Arellano, J., Durand, P, Hartogensis, O., Legain, D., Augustin, P., Gioli, B., Lenschow, D. H.,

ACPD
14, 32491–32533, 2014

Faloona, I., Yagüe, C., Alexander, D. C., Angevine, W. M., Bargain, E, Barrié, J., Bazile, E., Bezombes, Y., Blay-Carreras, E., van de Boer, A., Boichard, J. L., Bourdon, A., Butet, A., Campistron, B., de Coster, O., Cuxart, J., Dabas, A., Darbieu, C., Deboudt, K., Delbarre, H., Derrien, S., Flament, P., Fourmentin, M., Garai, A., Gibert, F., Graf, A., Groebner, J., Guichard, F., Jiménez, M. A., Jonassen, M., van den Kroonenberg, A., Magliulo, V., Martin, S., Martinez, D., Mastrorillo, L., Moene, A. F., Molinos, F., Moulin, E., Pietersen, H. P., Piguet, B., Pique, E., Román-Cascón, C., Rufin-Soler, C., Saïd, F., Sastre-Marugán, M., Seity, Y., Steeneveld, G. J., Toscano, P., Traullé, O., Tzanos, D., Wacker, S., Wildmann, N., and Zaldei, A.: The BLLAST field experiment: Boundary-Layer Late Afternoon and Sunset Turbulence, Atmos. Chem. Phys., 14, 10931–10960, doi:10.5194/acp-14-10931-2014, 2014. 32494, 32496, 32497, 32499, 32502, 32508

Meneveau, C. and Katz, J.: Scale-invariance and turbulence models for large-eddy simulation, Annu. Rev. Fluid Mech., 32, 1–32, 2000. 32507

Moeng, C. H.: A large-eddy-simulation model for the study of planetary boundary-layer turbulence, J. Atmos. Sci., 41, 2052–2062, 1984. 32499

Moeng, C.-H. and Wyngaard, J.: Spectral-analysis of large-eddy simulations of the convective boundary-layer, J. Atmos. Sci., 45, 3573–3587, 1988. 32514

Monin, A. and Yaglom, A.: Statistical Fluid Mechanics, vol. 2, edited by: Lumley, John L., The MIT Press, Massachussets, 1975. 32494

Nadeau, D., Pardyjak, E., Higgins, C., Fernando, H., and Parlange, M.: A simple model for the afternoon and early evening decay of convective turbulence over different land surfaces, Bound.-Lay. Meteorol., 141, 301–324, doi:10.1007/s10546-011-9645-x, 2011. 32494, 32496

Nieuwstadt, F. T. M. and Brost, R. A.: The decay of convective turbulence, J. Atmos. Sci., 43, 532–546, 1986. 32494, 32495, 32514

Patton, E. G., Sullivan, P. P., and Moeng, C. H.: The influence of idealized heterogeneity on wet and dry planetary boundary layers coupled to the land surface, J. Atmos. Sci., 62, 2078–2097, 2005. 32499

Pietersen, H., Vilà-Guerau de Arellano, J., Augustin, P., de Coster, O., Delbarre, H., Durand, P., Fourmentin, M., Gioli, B., Hartogensis, O., Lothon, M., Lohou, F., Pino, D., Ouwersloot, H. G., Reuder, J., and van de Boer, A.: Study of a prototypical convective boundary layer observed during BLLAST: contributions by large-scale forcings, Atmos. Chem. Phys. Discuss., 14, 19247–19291, doi:10.5194/acpd-14-19247-2014, 2014. 32499

ACPD
14, 32491–32533, 2014

Pino, D., Jonker, H., Vilà-Guerau De Arellano, J., and Dosio, A.: Role of shear and the inversion strength during sunset turbulence over land: characteristic length scales, Bound.-Lay. Meteorol., 121, 537–556, doi:10.1007/s10546-006-9080-6, 2006. 32494, 32495, 32502, 32513, 32514

Rizza, U., Miglietta, M. M., Acevedo, O. C., Anabor, V., Degrazia, G. a., Goulart, A. G., and Zimmerman, H. R.: Large-eddy simulation of the planetary boundary layer under baroclinic conditions during daytime and sunset turbulence, Meteorol. Appl., 20, 56–71, doi:10.1002/met.1284, 2013. 32494

Saïd, F., Corsmeier, U., Kalthoff, N., Kottmeier, C., Lothon, M., Wieser, A., Hofherr, T., and Perros, P.: ESCOMPTE experiment: intercomparison of four aircraft dynamical, thermodynamical, radiation and chemical measurements, Atmos. Res., 74, 217–252, doi:10.1016/j.atmosres.2004.06.012, 2005. 32497

Shaw, W. and Barnard, J.: Scales of turbulence decay from observations and direct numerical simulation, in: 15th Symposium on Boundary Layers and Turbulence, 8.3, Wageningen University, The Netherlands, 2002. 32508

Sorbjan, Z.: Decay of convective turbulence revisited, Bound.-Lay. Meteorol., 82, 501–515, 1997. 32494, 32495, 32513, 32514

Sullivan, P. P. and Patton, E. G.: The effect of mesh resolution on convective boundary layer statistics and structures generated by large-eddy simulation, J. Atmos. Sci., 68, 2395–2415, doi:10.1175/JAS-D-10-05010.1, 2011. 32499, 32500

Vilà-Guerau de Arellano, J., Dosio, A., Vinuesa, J.-F., Holtslag, a. a. M., and Galmarini, S.: The dispersion of chemically reactive species in the atmospheric boundary layer, Meteorol. Atmos. Phys., 87, 23–38, doi:10.1007/s00703-003-0059-2, 2004. 32494

ACPD
14, 32491–32533, 2014

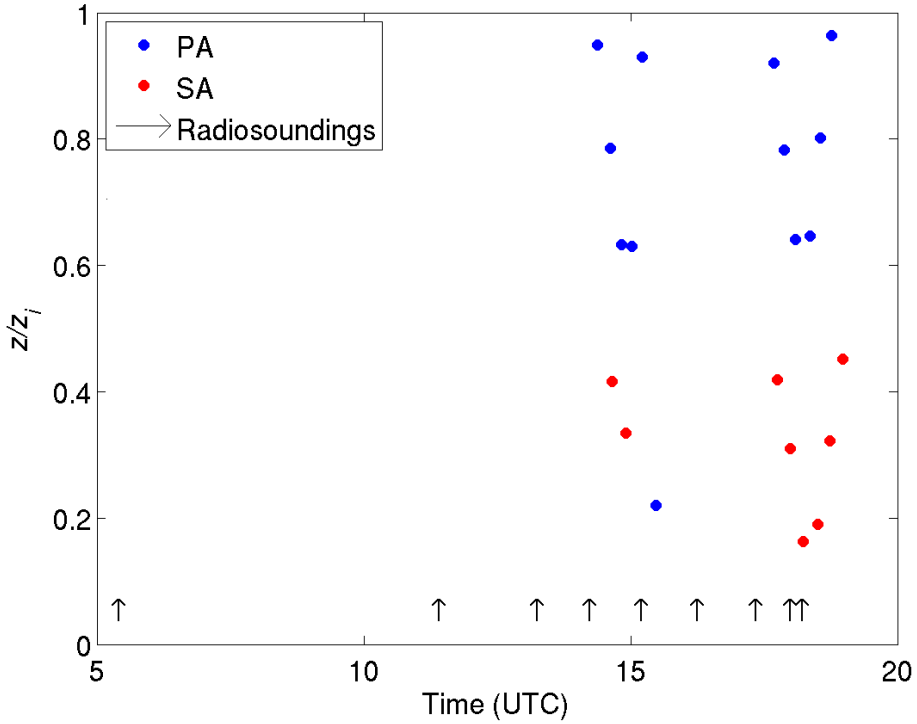

Figure 1. Normalized altitude z/z_i (where z_i is the PBL depth) of the legs flown by the two aircraft the 20 June 2011 (Piper Aztec in blue, Sky Arrow in red) and launching times of the radiosoundings (black arrows).

ACPD
14, 32491–32533, 2014

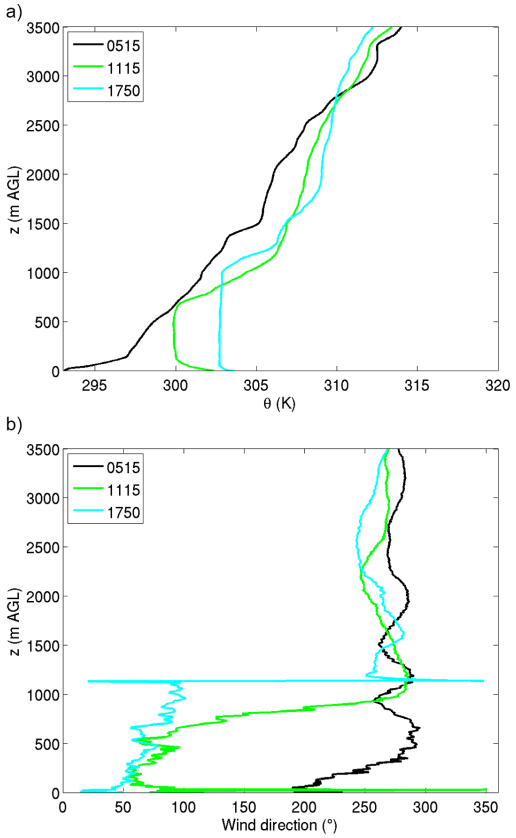

Figure 2. Observed vertical profiles of **(a)** the potential temperature θ and **(b)** the wind direction on the 20 June 2011.

ACPD
14, 32491–32533, 2014

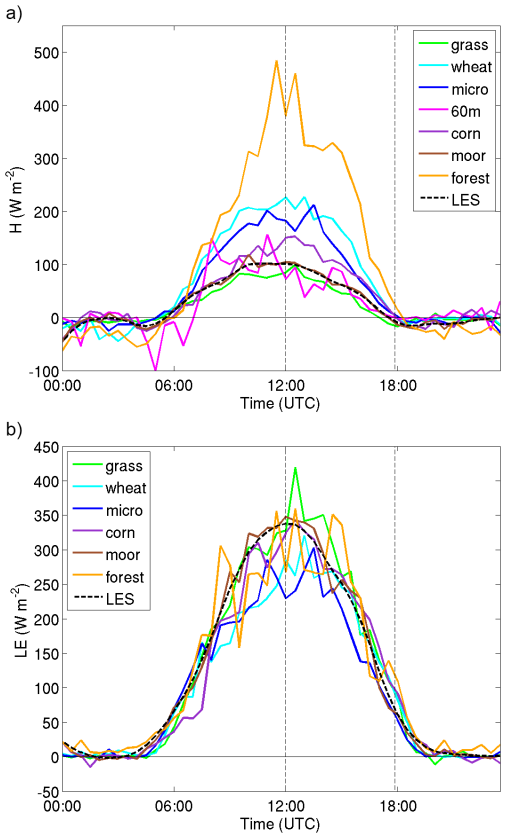

Figure 3. Temporal evolution of **(a)** surface sensible (H) and **(b)** latent (LE) heat fluxes over several vegetation coverages, on 20 June 2011. Dashed black curves stand for the surface flux used as boundary conditions for the LES. The vertical dashed lines stand for the times of maximum surface buoyancy flux (at 12:00 UTC) and zero value (at 17:50 UTC).

ACPD
14, 32491–32533, 2014

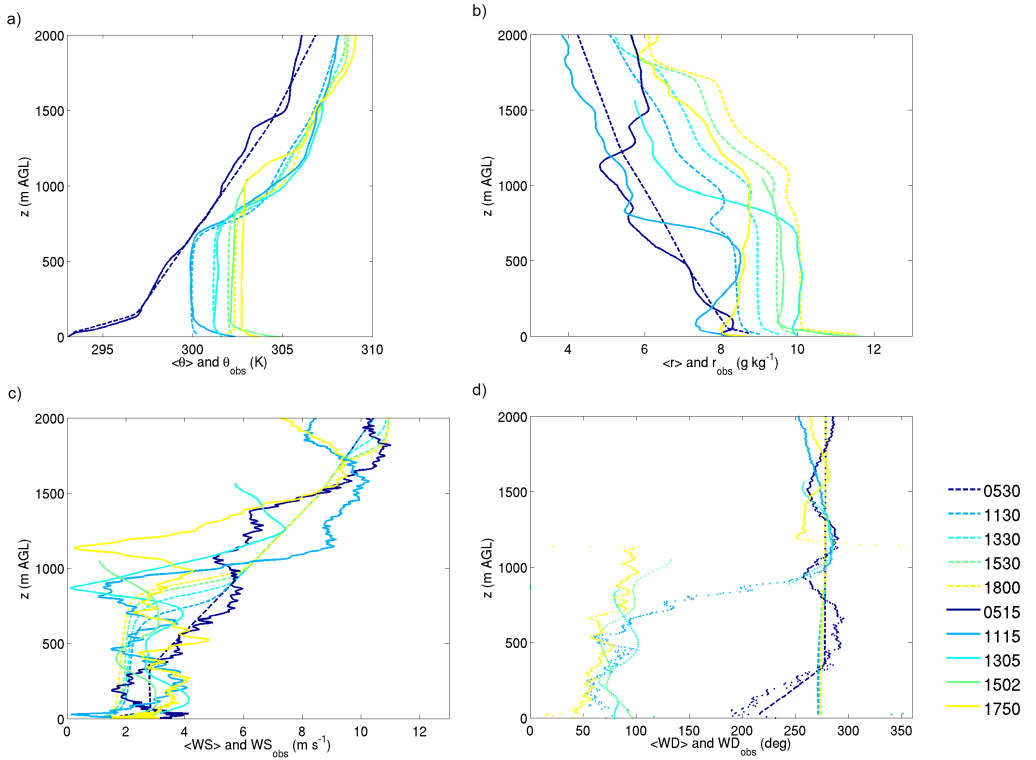

Figure 4. Vertical profiles of **(a)** θ, **(b)** r, **(c)** wind speed (WS), **(d)** wind direction (WD) observed (solid lines and dotted lines for WD) and obtained by LES (dashed lines).

ACPD
14, 32491–32533, 2014

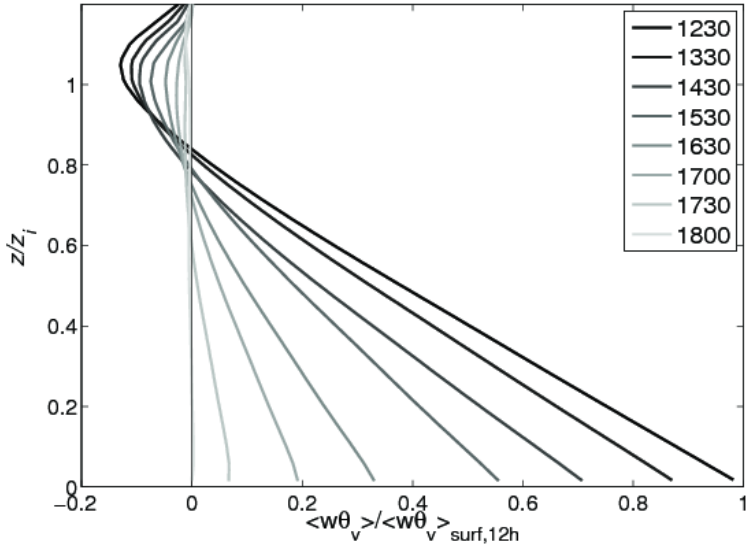

Figure 5. Vertical profiles of the buoyancy flux normalized by the surface buoyancy flux at 12:00 UTC according to the normalized height z/z_i.

ACPD
14, 32491–32533, 2014

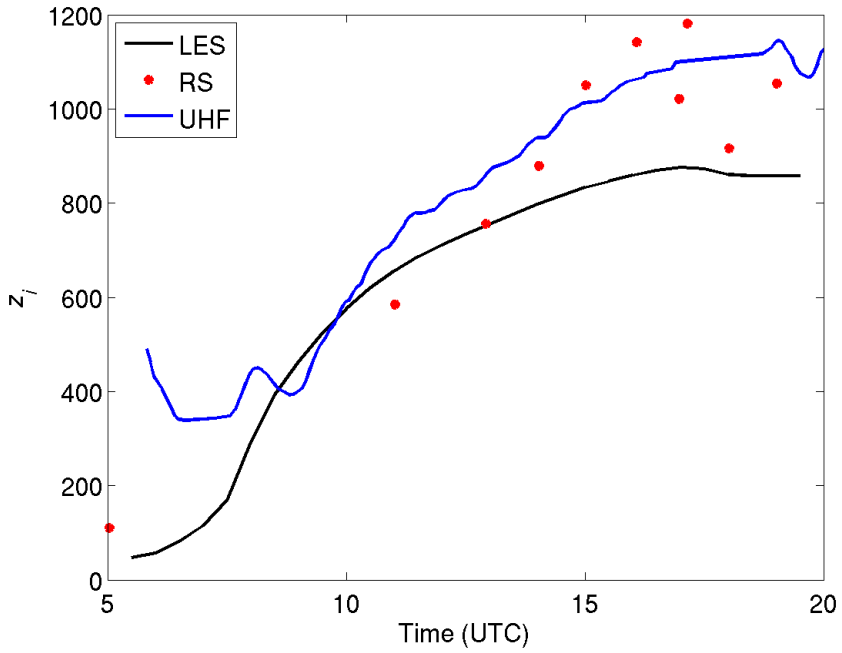

Figure 6. Temporal evolution of z_i in the simulation (black), observed by the UHF wind profler (blue) and depicted using radiosondes (RS) measurements (red dots).

ACPD
14, 32491–32533, 2014

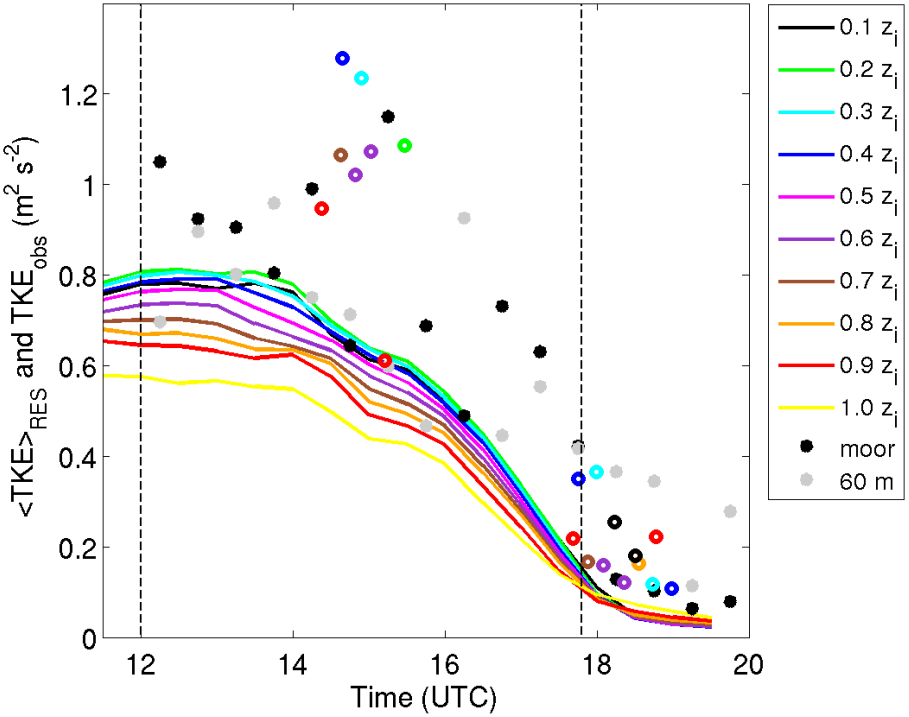

Figure 7. Temporal evolution of the resolved TKE (subscript RES) at different heights in the simulation (different colors). TKE deduced from aircraft and surface (subscript OBS) spectra integrated over the LES spectra wavenumber range (open and filled circles, respectively). The vertical dashed lines stand for the times of maximum surface bouyancy flux (at 12:00 UTC) and its zero value (at 17:50 UTC).

ACPD
14, 32491–32533, 2014

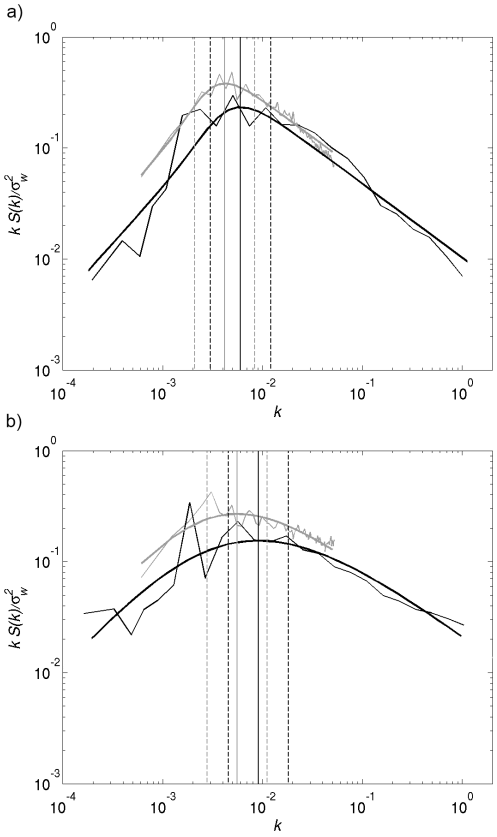

Figure 8. Normalized w spectra at **(a)** 15:00 and **(b)** 18:00 UTC from both aircraft (black) and LES (grey), fitted with the KL89 analytical spectral model (thick lines). The vertical continous line represent Λ_w, the maximum energy wavenumber and the dashed vertical lines represent k_1 and k_2, the limits of the low wavenumber range and of the inertial subrange, defined as $k_1 = \pi/\Lambda_w$ and $k_2 = 4\pi/\Lambda_w$.

ACPD
14, 32491–32533, 2014

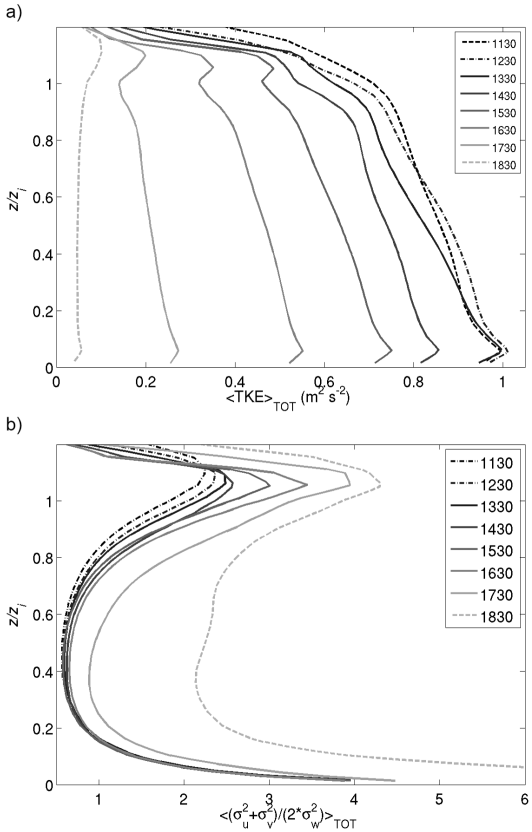

Figure 9. Vertical profiles of the total (resolved and subgrid (subscript TOT)) **(a)** TKE and **(b)** anisotropy at several hours during the AT in the LES.

ACPD
14, 32491–32533, 2014

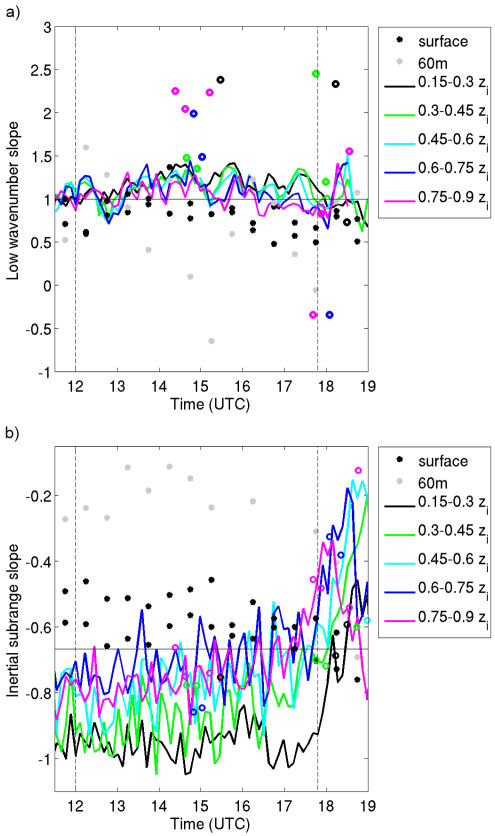

Figure 10. Temporal evolution of the slopes in **(a)** the low wavenumber range and **(b)** the inertial subrange of the *w* spectra obtained by LES (continuous lines), aircraft and surface measurements (open and filled circles) at different heights (colors). The horizontal black lines stand for the theoretical expected values

ACPD
14, 32491–32533, 2014

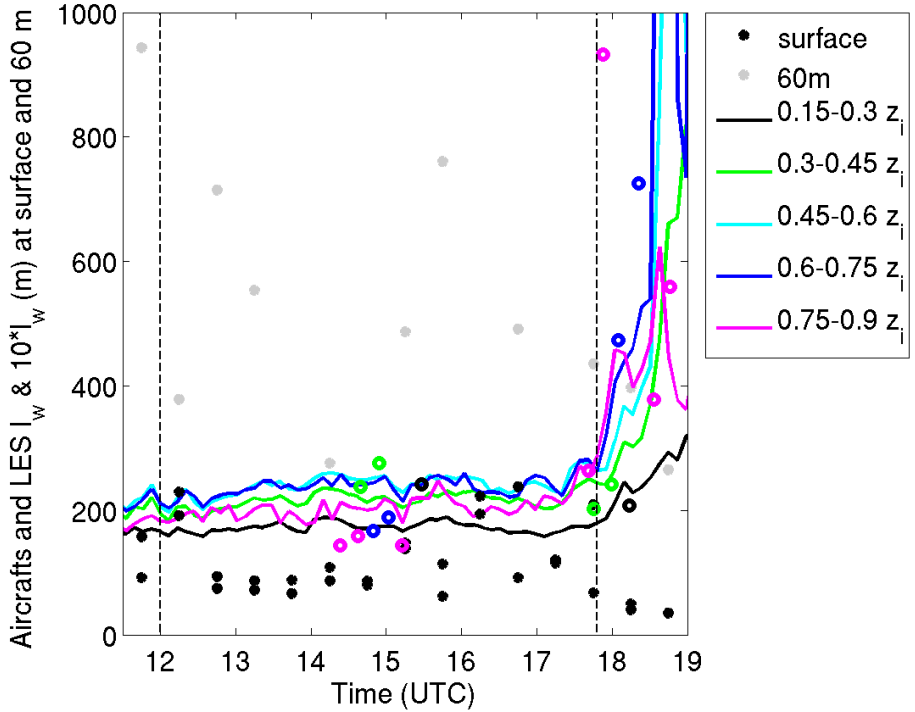

Figure 11. Temporal evolution of l_w calculated from the KL89 analytical model fit on LES (continuous lines), aircraft (open circles) and surface (closed circles) spectra at different heights (different colors). Note that l_w at surface and at 60 m are multiplied by a factor 10. The vertical dashed lines stand for the times of maximum surface bouyancy flux (at 12:00 UTC) and its zero value (at 17:50 UTC).

ACPD
14, 32491–32533, 2014

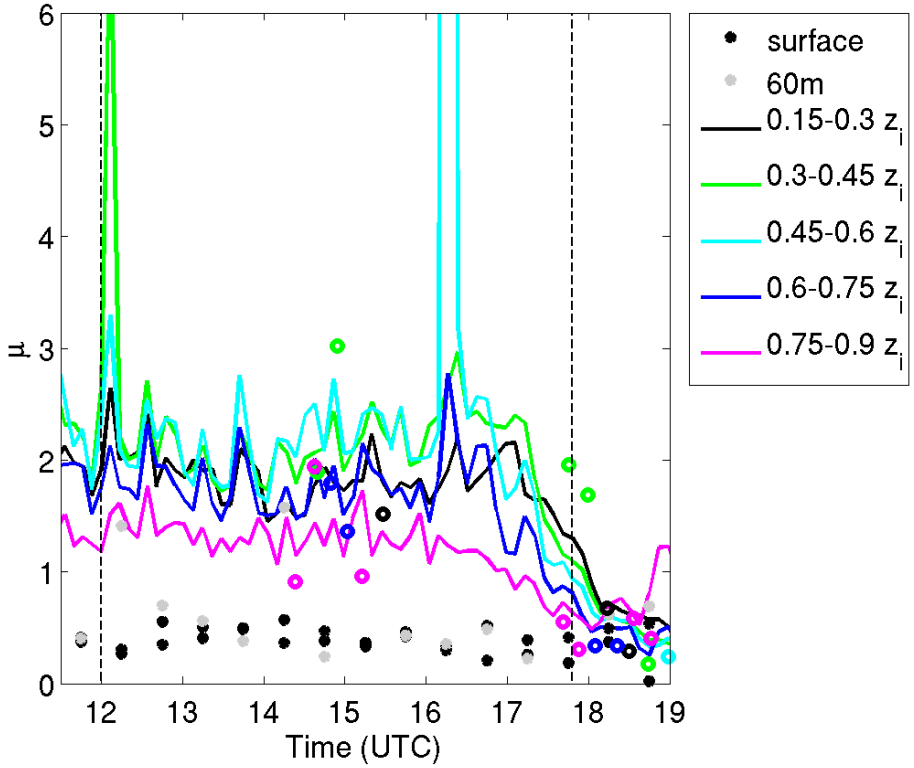

Figure 12. Temporal evolution of the parameter μ, obtained from the KL89 analytical model, by using LES (continous lines), aircraft (open circles) and surface (closed circles) data. The vertical dashed lines stand for the times of maximum surface bouyancy flux (at 12:00 UTC) and its zero value (at 17:50 UTC).

ACPD
14, 32491–32533, 2014

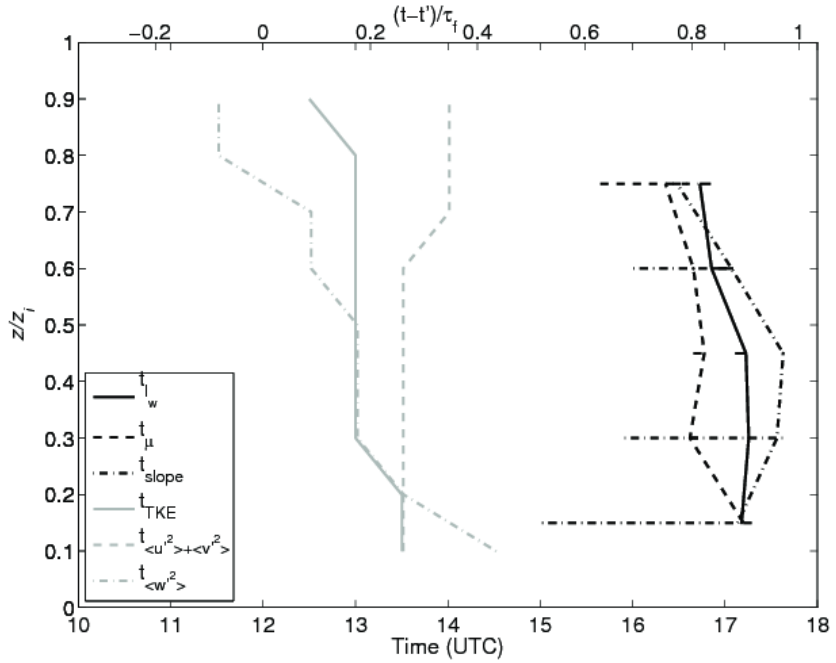

Figure 13. Vertical profiles of the timings of changes observed in the evolution of the TKE, the vertical and horizontal variances, l_v, μ and the inertial subrange slope of w spectra. t' is defined as the time when H is maximum (i.e. at 12:00 UTC).

ACPD
14, 32491–32533, 2014